Refined Method for Determining Adhesive Forces of Dust on Aerospace Materials

Joshua H. Litofsky[1], Sonali R. Nagpal[2], Amy M. Fritz[3], Chandler S. Lawson[4], Raj R. Gohil[5], Courtney A. Steagall[6], Ryunosuke Greer[7], Kenton R. Fisher[8]
National Aeronautics and Space Administration, Houston, Texas, 77058

Alejandro D. Rincón[9], Jeremy A. Wilson[10], Michael E. Urrutia[11]
Amentum, Houston, Texas, 77058

and

Ronald G. Lee[12], Edward Rosenthal[13]
Booz Allen Hamilton, Houston, Texas, 77058

In this study, we expand upon a method of quantifying the adhesive force of lunar simulant under simulated lunar surface conditions. This technique applies a monolayer of dust to a small sample coupon which is then rapidly rotated; from the size of the simulant grains that remain on the sample coupon, the adhesive force of the simulant can be calculated. These tests, using lunar simulant JSC-1A across 16 different sample coupon materials, were performed under vacuum and exposure to ultraviolet light to simulate lunar conditions. This study demonstrates the ease and high throughput with which adhesive forces can be experimentally determined under lunar conditions across a wide variety of materials. Improvements upon previous attempts at quantifying forces of adhesion are shown, including the addition of an applied acceleration force degree of freedom and the ability to test multiple different materials at the same time. Deliverables from this test include quantitative and experimentally determined adhesive forces for use in dust transport and analysis models as well as qualitative metrics to directly compare the susceptibility of materials to lunar dust adhesion. Included forward work outlines hardware upgrades to improve simulant application homogeneity and in-situ simulant particle size analysis.

Acronyms and Nomenclature

ACE = Advanced Concepts for Exploration

[1] Aerospace Technologist – Technical Management, Engineering Directorate, 2101 E NASA Pkwy, Houston, TX 77058
[2] Aerospace Engineer, Engineering Directorate, 2101 E NASA Pkwy, Houston, TX 77058
[3] Aerospace Technologist – Aerospace Flight Systems, Engineering Directorate, 2101 E NASA Pkwy, Houston, TX 77058
[4] Space Scientist, Aerospace Technologist – Planetary Studies, Exploration Architecture, Integration, and Science Directorate, 2101 E NASA Pkwy, Houston, TX 77058
[5] Student Trainee, Engineering Directorate, 2101 E NASA Pkwy, Houston, TX 77058
[6] Aerospace Technologist – Structural Materials, Engineering Directorate, 2101 E NASA Pkwy, Houston, TX 77058
[7] Student Trainee, Engineering Directorate, 2101 E NASA Pkwy, Houston, TX 77058
[8] Aerospace Technologist – Planetary Studies, 2101 E NASA Pkwy, Houston, TX 77058
[9] Systems Engineer, Lunar Dust Mitigation, JE16, 2224 Bay Area Boulevard, Houston, TX 77058
[10] Mechanical Design Engineer, JE13, 2224 Bay Area Boulevard, Houston, TX 77058
[11] Project/Test Engineer, JE30, 2224 Bay Area Boulevard, Houston, TX 77058
[12] Gateway Cis-Lunar Dust Transfer Modeling and Analysis Task Lead, 2525 Bay Area Blvd, Houston, TX 77058
[13] Gateway Cis-Lunar Dust Transfer Modeling and Analysis Scientist, 2525 Bay Area Blvd, Houston, TX 77058

CAD	=	computer-aided design
GOLDMAP	=	Gateway On-orbit Lunar Dust Modeling and Analysis Program
HLS	=	Human Landing System
JSC	=	Johnson Space Center
N/cm^2	=	newtons per centimeter squared
NASA	=	National Aeronautics and Space Administration
RPM	=	rotation per minute
SDL	=	Simulant Development Lab
UV	=	ultraviolet

I. Introduction

Lunar dust has been shown to have high forces of adhesion across a wide array of aerospace materials, including coated and uncoated metals, glasses, and polymers, among others [1, 2, 3]. It is well known that this dust can cause hazards and other off nominal effects through a variety of mechanisms, including aerosol ingestion, abrasion, optical and thermal changes, mechanical hindrance of mechanisms and seals, and stochastic electrostatic effects [4]. As such, it is important to understand where and how much dust will adhere to the various systems, subsystems, and components on future lunar surface missions. Lunar dust, particularly the component that is less than 50 microns in diameter, will be airborne for a substantial period, and thus will be able to travel and adhere across many different surfaces and materials in both the interior and exterior of vehicles within throughout the entirety of the lunar surface mission architecture, not only limited to those on the surface, such as the Human Landing System, or HLS. This test, measuring particle adhesion through centripetal force mass shedding, was developed and refined to accurately quantify the adhesive force of lunar simulant in environmentally representative conditions across an array of aerospace materials to inform lunar dust modeling efforts, such as the Gateway On-orbit Lunar Dust Modeling and Analysis Program GOLDMAP [1, 5, 6, 7]. The results of this test can be used for GOLDMAP and other modeling and analysis efforts, as well as provide a framework from which to build other lunar dust adhesion and environment studies.

II. Centripetal Force Mass Shedding Experimental Details

This test utilizes centripetal force mass shedding to determine the adhesive force between lunar simulant and a variety of aerospace materials in a similar fashion to Dove and Barker, as well as others [1, 6]. Multiple samples were loaded into a vertically rotating cylinder that, through applications of increasing acceleration loads, ejected dust as a function of this applied load. The samples, having ejected some particles while retaining others, were then examined by optical microscopy to determine particle size and the resulting adhesive forces. The simulant application and its ejection were fully performed under vacuum in a vacuum chamber; some tests were additionally performed while under UV exposure. While the electrostatic environment was not quantified, it is expected that the lunar simulant underwent some charging during its application. The following sections detail the hardware and experimental setup.

A. Testing hardware and control

This hardware was developed based on known and existing hardware from Barker [1]. The primary goal, as was that from Barker, was to develop a method to controllably rotate a sample at a known speed. Additional capabilities that were added to this hardware included the ability to control the simulant deposition as well as the automated transition remotely and reliably between the hardware's "dusting" configuration and its "testing" configurations. These capabilities were added to ensure full and repeatable simulant application. The CAD models that demonstrate the hardware in its dusting configuration and its testing configuration are shown in Figure 1a and 1b, respectively.

1. Hardware

This hardware was developed to replicate the work done by Barker with some marked improvements. These improvements revolve around the ability to precisely apply simulant under vacuum while keeping the most of the hardware's usage the same. The elegance of the Barker hardware was its ability to eject simulant quickly and easily under vacuum while maintaining a small physical and electrical footprint. The current design builds upon existing CREO CAD models from Barker and used 3D printing for both prototyping and fabrication. Existing metal fabrications were used when present. All 3D printed materials were printed from Ultem, a low-offgassing material regularly used in vacuum applications.

The metal baseplate and glass shield were reused from the previous tests. Added to this baseplate are the two primary components of the testing apparatus: the simulant application mechanism and the sample control mechanisms. The simulant application tower includes a stainless-steel machined base upon which sits the shaker arm assembly. The

shaker arm consists of 3 main parts: a machined stainless-steel sieve holder, a stepper motor that swings the shaker arm in and out of simulant deposition configurations, and a set of push/pull solenoids that shake the sieve holder back and forth. The solenoid pair is controlled from an Arduino by the hardware operator. Two sieves are loaded and taped into the sieve holder; the top is a #230 sieve while the bottom is a #325 sieve; the bottom size is selected to apply simulant that is no larger than 45 microns, while two sieves were used to ensure fuller simulant coverage. Bounding the movement of the shaker arm is a 3D printed hard stop. This hard stop is in place to prevent the arm from moving out of position and providing a location from which to zero the stepper motor.

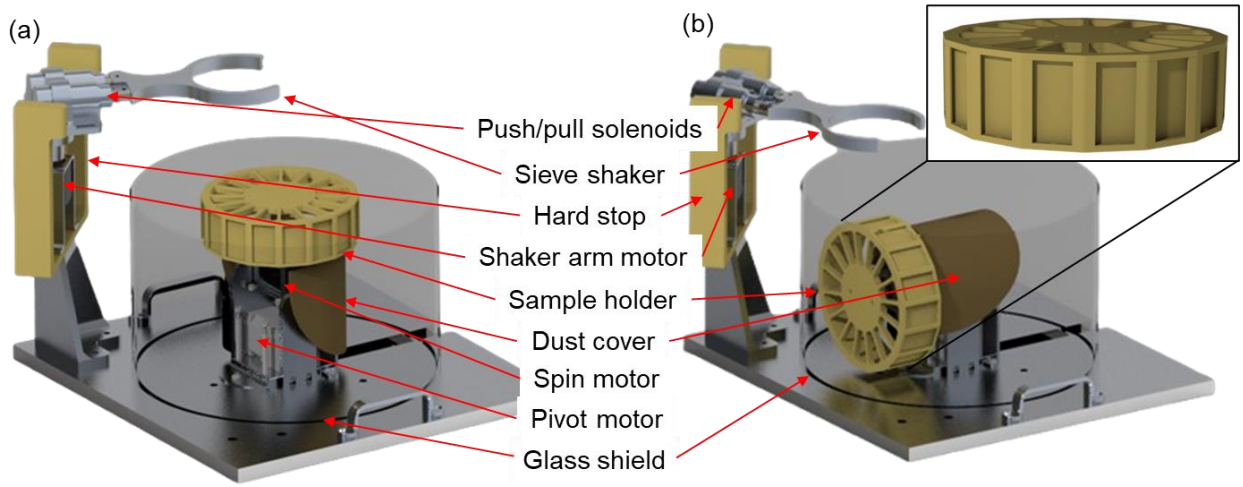

Figure 1. CAD design of the lunar dust adhesion testing hardware in its dusting (a) and testing (b) configurations. Critical components of the hardware have been labeled, and the sample holder is shown in the upper right inset. Samples are loaded into the 16 slots around the edge of the sample holder.

The other component of the testing apparatus is the sample control mechanism. There are two primary functions of this mechanism: 1) to pivot the samples down and up into and out of the simulant application configuration and the simulant ejection configuration; and 2) to spin the sample holder, and therefore the samples, in both the application and ejection configurations. A machined stainless-steel mount was screwed into the existing metal baseplate. Attached to this mount is the "pivot" stepper motor; this motor is responsible for moving the apparatus between the testing and application configurations. On the pivot motor is the housing and "spinner" stepper motor; this motor is responsible for rotating the sample during simulant application and testing. To avoid simulant contamination of the motors, a 3D printed simulant shield was affixed to the upward facing side of the testing apparatus. Controls for the pivot and spinner motors were fed underneath the apparatus and below the glass shield. A photointerruptor was installed on the top of the testing apparatus to measure the passing of the sample holder to validate rotational speed was correct prior to the test.

The sample holder was a 16-sided, 3D printed apparatus approximately 6" in diameter. Each side of the sample holder is designed to hold a 1.5 x 3 cm sample coupon. The samples can slide into the notch on each of the sides of the sample holder, and then the top of the sample holder is screwed on to ensure the samples do not move during testing. A small opening is present at the bottom of each sample holder notch to allow for the samples to be pushed up using a tool to aid the removal process.

2. Software and controls

Building upon existing software, the controls all three motors used a Zaber X-MCB1 Stepper Motor Controller (National Instruments) USB-6001 Multifunction I/O Data Acquisition Device with modified LabView control software. Both the control interface for the 3 stepper motors and the rotational speed from the photointerruptor were contained in the LabView software. The software control allowed for left/right movement of the shaker motor, up/down movement of the pivot motor, and full rotational control of the spinner motor; this rotational control includes speed, acceleration, and run time of the spinner motor. The solenoids for the sieve shaker were controlled through interfacing with an Arduino board.

B. Vacuum testing

Hardware verification and testing occurred in the Advanced Concepts for Exploration (ACE) Lab dirty vacuum chamber in Building 36 at NASA's JSC. This chamber is a 2' x 2' x 2' fully modular vacuum chamber from Ideal Vacuum Products. Tests were run at approximately 10^{-6} Torr after approximately a 30-minute pump down time. Tests were run both at standard vacuum conditions and then again at standard vacuum conditions and under UV exposure. The chamber and test articles within were under UV exposure during chamber evacuation, simulant application, and simulant ejection; this total time is approximately 45 minutes and was the same for all tests. UV exposure, at a wavelength of 190 nm (corresponding to 6.53 eV), was applied using two UVB-100 lamps obtained from RBD Instruments. The lamps were mounted to CF flanges installed on the vacuum chamber. Images of the chamber are shown in Figure 2.

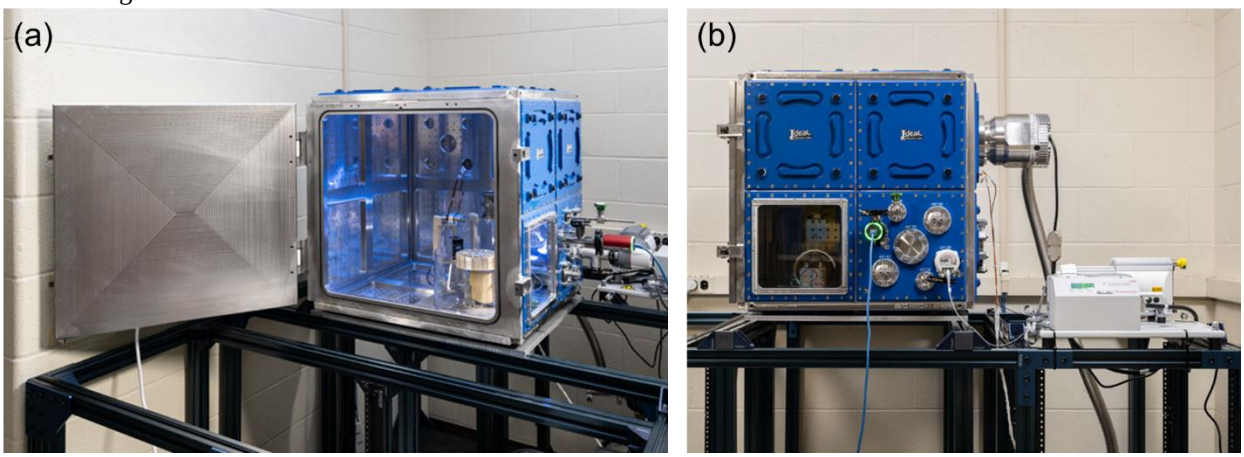

Figure 2. Images showing the ACE Lab dirty vacuum chamber with the hardware loaded. Two views are shown: the interior (a); and exterior (b).

Each sample was cleaned with an isopropanol wipe prior to usage. Upon drying, the sample was then weighed in the Simulant Development Lab (SDL) in Building 36 at JSC. The samples were loaded into the sample holder 8 at a time; the pivot motor was not reliable to be raised and lowered at a full 16-sample loading. The sample holder was placed on the D-shaft of the spinner motor. Prior to closing the doors and pulling vacuum, a full functionality test was performed; this test included ensuring that the sample spinner could spin, the sieve shaker could shake and apply dust, and the pivot motor could be raised and lowered. After successful completion of the systems check, the vacuum chamber was closed, and vacuum was pulled. Upon reaching approximately 10^{-2} Torr, simulant application was induced. Simulant application was performed with 60 Hz sieving across 2 rotations of the sample spinner at 15 rpm. These variables were selected to apply the most uniform simulant at approximately 30% surface area coverage. This surface area coverage minimizes simulant cohesion which helps prevent the loss of simulant from dust "avalanching" [8].

Preliminary tests were performed to ensure a high degree of repeatability of simulant deposition between runs. Verification steps included loading one sample into the chamber, evacuating the chamber to simulant application levels, and then applying simulant to the sample in the nominal fashion. The chamber was then pressurized, and the samples were removed from chamber and sample holder and transported to the SDL where the percent area coverage was calculated (see Section II.C). This run was performed twice more for a total of three runs. These tests found that the percent area coverage of the sample was consistent to within 5% of the average surface area coverage (32%). These data validated our hardware to repeatably perform the application of simulant.

Upon completion of the simulant deposition, the turbo pump was turned on and the chamber was brought down to approximately 10^{-6} Torr. The sample holder was then pivoted up into testing configuration and accelerated to the test's desired rotational speed. After holding the speed for 10 seconds, the samples were slowed to a stop and the chamber was returned to atmospheric pressure. The sample holder was then removed and had its samples extracted. Care was taken as to not jostle the samples during removal or transport to minimize incidental dust ejection. Visual inspection indicated that minimal dust was lost during sample removal from the sample holder and further transport. Because the samples had already experienced vibratory and acceleration loads, the nominal loads applied during unloading and transport did not appear sufficient as to remove or eject existing adhered dust from the sample coupons. A small but uncharacterized quantity of dust was found to have adhered to the lids of the plastic sample containers during transport.

Total transport time from removal of the sample holder to placing sample next to the scale was less than 30 seconds. The coupons were then weighed in the SDL and brought to a digital microscope for particle size analysis. Upon completion of the microscopy, the samples were cleaned with isopropanol wipes and weighed for the next test.

Test rotational speeds were predetermined based on resultant acceleration forces (Table 1); a 0 RPM case was also analyzed. The ramp up and slow down accelerations to and from the desired rotational speeds were 25 RPM per second and 50 RPM per second, respectively.

Table 1. Rotation speeds and resultant acceleration forces used during the test

Rotation speed	Acceleration force (G's)
30	0.05
297	5.01
420	10.02
664	25.04
930	49.12
1327	100.01
1877	200.09

C. Particle size analysis

Particle size analysis was performed after each applied acceleration. Particle sizes were determined by a Keyence VHC-7000 Series Digital Microscope in the SDL. The Keyence Digital Microscope is a fully automated 4k Ultra-High Accuracy Microscope with a fully integrated head that accommodates smooth magnification transitions from 20x to 1000x. Samples were loaded individually onto the Keyence sample stage and examined at 800x magnification at 3 locations: left third of the sample; middle third of the sample, and right third of the sample. Using the Keyence software and its particle detection algorithm, the quantity, size, and shape of the particles were calculated across the three locations. Through preliminary informal testing, the Keyence particle detection algorithm was seen to be as accurate as other third-party software, such as ImageJ. The 800x magnification allows for the for the detection and quantification of submicron particles while avoiding edge effects that occur at the 1000x magnification. An example of this analysis can be seen in Figure 3.

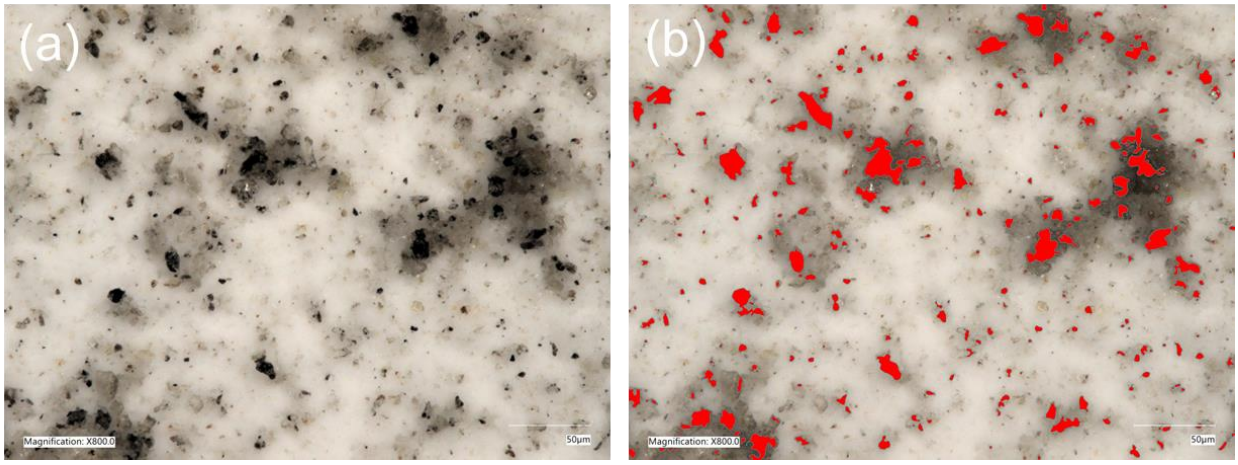

Figure 3. Microscopy at 800x of JSC-1A on Z93C55 painted aluminum (a). Particles detected and shaded by the Keyence software and particle detection algorithm (b).

As seen above, most particles are adhered in a non-continuous monolayer across the sample. Visual inspection of the micrographs does not immediately show significant stacking or cohesion of simulant particles. However, there are some apparent "clumps" of simulant. The Keyence software can nominally distinguish between overlapping particles, allowing for more accurate single-particle characterization. Some manual adjustments are performed to allow for the most accurate particle separation and identification. Additionally, while most substrates provided enough natural contrast with the JSC-1A simulant, some substrates did not and various adjustments using the Keyence software were

performed. These adjustments included modulating the digital contrast or brightness, changing the lighting brightness, digitally removing texture, and adjusting the angle and location from which the sample was lit.

Percent area coverage was also calculated using the digital microscope. At 200x, the same particle detection algorithm was used, but the microscope's "area ratio" figure provided the percent area coverage. This figure is the ratio of the area of the image covered by particles to that uncovered by particles. The magnification 200x was used to image the widest region possible, and three areas (left third, middle third, and right third) were again examined.

D. Test materials

1. Samples

Sixteen sample materials were selected as being potentially used on the lunar surface and in orbit. Materials selected for use in orbit are anticipated to come in contact with lunar dust upon transfer from HLS to Gateway or other orbiting vehicles. These materials are listed below.

1. Silver-coated Teflon
2. 6061 aluminum
3. Aluminized Kapton
4. Anodized aluminum
5. Beta cloth
6. Germanium black Kapton
7. Kapton
8. Magnesium fluoride-coated cerium doped glass
9. Orthofabric
10. Borosilicate glass doped with cerium dioxide, substrate silverized and overcoated with corrosion protective layer
11. Silicone
12. 304 passivated stainless steel
13. Stamat black Kapton
14. 6-4 titanium
15. Tiodize type II-coated titanium
16. Z93C55-painted aluminum

While not encompassing all materials that will experience lunar dust loads on or above the lunar surface, this selection aims to sample a wide range of material types (metals/alloys, coatings, softgoods, soft materials, thin films, and electronic components).

Most samples were either machined to 1.5 cm x 3 cm and with a chamfer on their long edges or were adhered to bare aluminum. Samples such as the Kapton needed a rigid backing to be loaded into the sample container. While it has been shown that underlying materials can affect the properties of the top layer, it is not anticipated that this effect would be large enough to have necessitated a different loading mechanism [6]. The silicone samples were cut to 1.5 cm x 3 cm and then loaded directly into the sample holder without a chamfered edge.

2. Simulant

JSC-1A was selected as the lunar dust simulant for this experiment for a variety of reasons, the primary of which was to keep consistency with previous test campaigns [1]. Additionally, its primarily gray colors provided decent contrast against most, though not all, of the sample materials. This simulant is also very well characterized and has a long history of usage for adhesion tests [9, 10, 11, 1, 6]. The simulant was sieved to 45 microns prior to usage to align with experimentally determined particle sizes of expected dust that has ingressed into HLS and other vehicles [12]. The simulant had undergone a 24-hour bakeout at 120° C prior to usage and was stored in the vacuum chamber during testing. 3 g of simulant were placed in the top sieve for each run.

III. Analysis and simulant adhesive force calculation

The main goal of this work was to experimentally determine the adhesive force of lunar simulant under various conditions on numerous materials. To determine the adhesive force, an expanded force calculation was used:

$$F_a = ma = mr\omega^2 = 4\pi^2 s^{3/2} \rho_p f^2 r \tag{1}$$

where F_a is the adhesive force, m is the mass of the particle, a is the acceleration imparted from the rotating sample holder, r is the average radius of spin, ω is the angular velocity of the rotating sample holder at its average radius, s is the particle area, ρ_p is the bulk simulant density, and f is the rotation frequency. All variables are either known, such as the bulk simulant density, controlled, such as the rotation frequency and the average radius of spin, or experimentally determined, such as the particle surface area. The particle surface area is the one variable that is calculated from this experiment.

This force calculation was performed for all particles detected at every spin speed. Therefore, the adhesive force was determined as a function of sample material and applied acceleration; it is the addition of this second independent variable, applied acceleration, that allows for improved understanding on what particles are ejected during the full ramp up cycle.

Previous work only performed one force calculation after all accelerations were applied [1]. Using applied acceleration as an independent variable allows for the taking measurements during the ramp up cycle which was not previously performed. While this campaign's particle analysis measurements are not necessarily *in situ*, preliminary tests confirmed that the test-to-test variance was low enough to allow for this experimental design.

Some of the only dust adhesion data from lunar samples come from the returned Surveyor III surface sampler. Work by Scott and Zuckerman attempted to calculate the adhesive force of the lunar soil to the surface sampler scoop [13]. This work, along with work done in later years on lunar simulant, calculated the adhesive strength as the force per unit area [1]. Adhesion, both for particles and for general adhesives, is usually reported in this manner. Data for each applied acceleration on each material sample in both environmental conditions (vacuum and vacuum plus UV) are shown in Figure 4 and Figure 5. The data plotted in those figures are the adhesive force per unit area of the mean particle size for each data set. Data points that were associated with an incidental or unintentional loss of simulant during one or more phases of the experiment were removed.

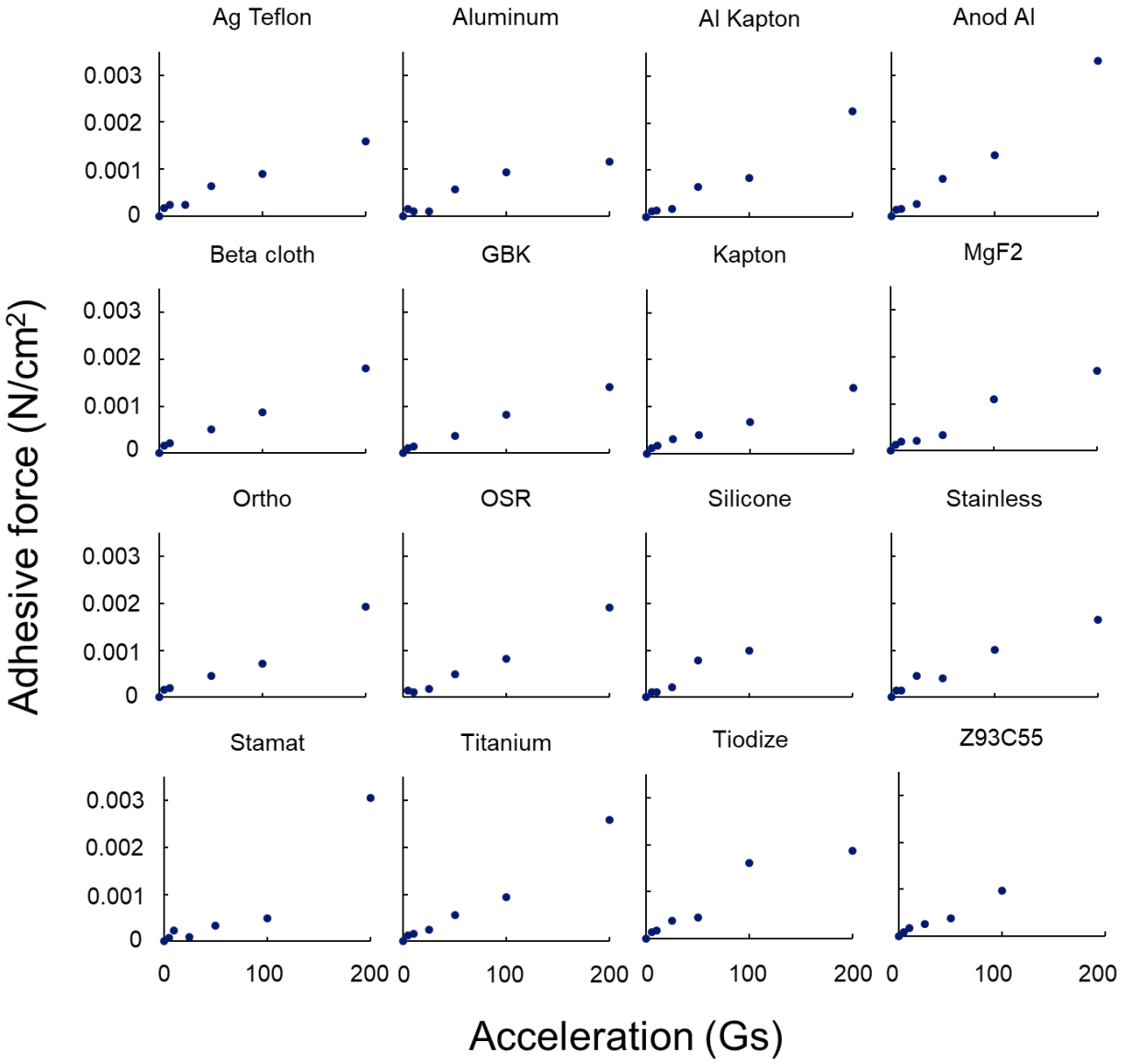

Figure 4. Adhesive force as a function of acceleration under vacuum conditions for the 16 material samples. Abbreviations are as follows: Ag Teflon - silver Teflon; Al Kapton - aluminized Kapton; Anod Al - anodized aluminum; GBK - germanium black Kapton; MgF2 - magnesium fluoride-coated cerium doped glass; Ortho - orthofabric; OSR - borosilicate glass doped with cerium dioxide, substrate silverized and overcoated with corrosion protective layer; Stamat - Stamat black Kapton; Tiodize - Tiodize type II-coated titanium; Z93C55 - Z93C55-painted aluminum

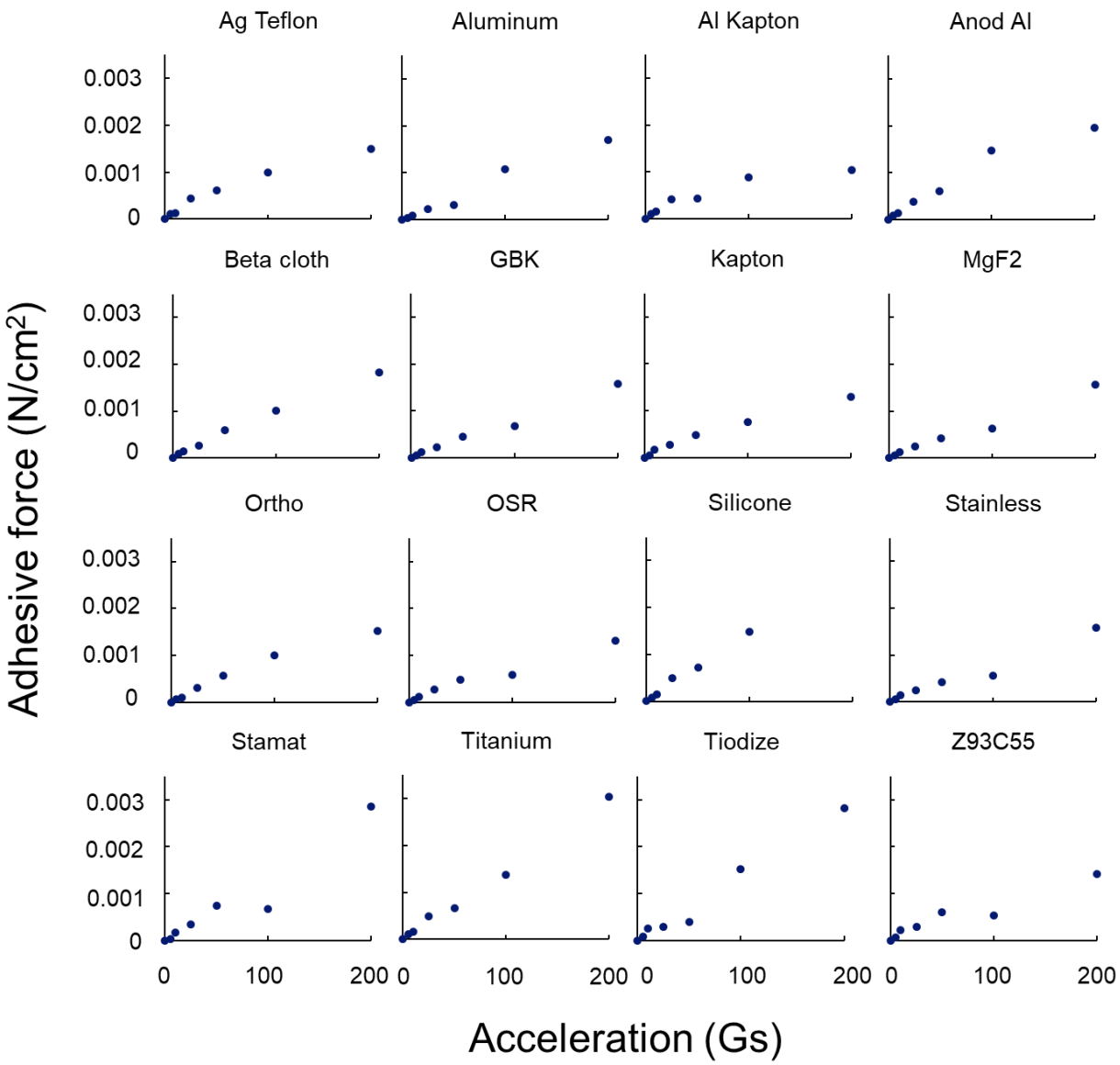

Figure 5. Adhesive force as a function of acceleration under vacuum plus UV conditions for the 16 material samples. Abbreviations are the same as in Figure 4.

The slope of the plots can provide a quantitative comparison between the different material samples; that is, those with a steeper slope are more adhesive to dust than those with shallower ones. These slopes were calculated as a line of best fit through the data; the goodness of fit ranged from 0.90 to 0.99. Additionally, the effect of the UV exposure on the simulant and the materials can be seen when comparing the slopes. Table 2 and Figure 6 shows these data across all samples. As seen in the chart, there is not an apparent consistent effect of the exposure to UV light. However, it should be noted that the similar patterns within materials have been seen in previous work [1]. For example, thermal-painted aluminum, such as Z93C55, has shown to have higher adherence to simulant under exposure to UV than without while bare aluminum has the reverse effect. More work is needed to explore these relationships in appropriate depth.

Table 2. Slopes of the adhesion force as a function of applied acceleration force as compared across both environments

Material	Vacuum	Vacuum + UV
Ag Teflon	7.6E-06	7.3E-06
Al	6.0E-06	8.9E-06
Al Kapton	1.1E-05	5.1E-06
Anod Al	1.6E-05	1.0E-05
Beta	8.6E-06	9.1E-06
GBK	7.0E-06	7.6E-06
Kapton	6.6E-06	6.3E-06
MgF2	8.6E-06	7.5E-06
Ortho	9.0E-06	7.7E-06
OSR	9.2E-06	6.2E-06
Silicone	1.7E-05	1.5E-05
Stainless	8.1E-06	7.4E-06
Stamat	1.4E-05	1.3E-05
Ti	1.2E-05	1.5E-05
Tiodize	9.9E-06	1.4E-05
Z93C55	9.4E-06	6.4E-06
Note: units are N cm^{-2} / G		

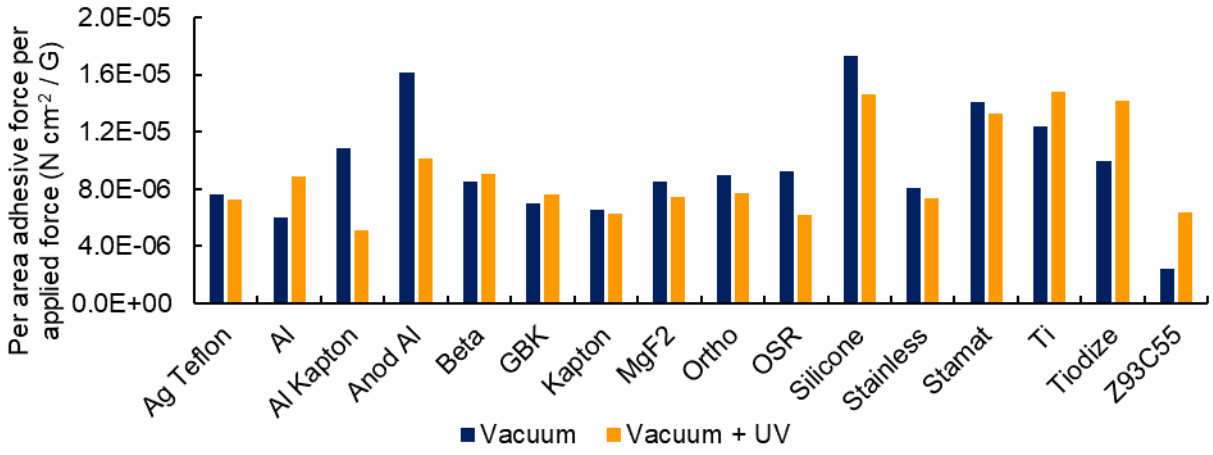

Figure 6. Slopes of the adhesion force as a function of applied acceleration force as compared across both environments (plotted from Table 2).

The last method presented in this work to quantify the adhesive force of lunar simulant is through the Hoekstra-Voight coefficient. This coefficient utilizes the mass difference between the material sample coupon after simulant has been applied (m_1) and after simulant ejection (m_0). When the ratio of m_1 to m_0 is plotted as a function of rotational frequency (RPM), the slope magnitude provides a direct method of comparing qualitative adhesive forces against one another without the need for image or microscopy analysis. The removal of this step decreases the cost and time of this method for calculating adhesive forces. Hoekstra-Voight coefficients are tabulated in Figure 7 alongside an example of this plot (Tiodize type II-coated titanium). Some materials do not have the Hoekstra-Voight coefficient calculated for one or both environments due to technical difficulties with weighing the sample.

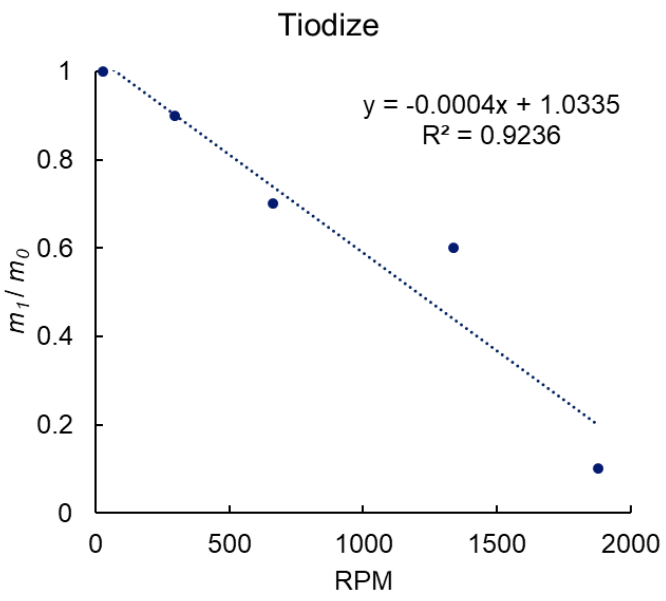

Material	Vacuum	Vacuum + UV
Ag Teflon	0.0005	0.0005
Aluminum	0.0006	0.0006
Al Kapton	0.0004	0.0005
Anod Al	0.0007	0.0007
Beta		0.001
GBK	0.0007	0.0025
Kapton	0.0012	0.0004
MgF2	0.0005	0.0004
Ortho	0.0007	0.0018
OSR	0.0005	0.0004
Silicone	0.001	0.0006
Stainless	0.0006	0.0005
Stamat	0.0004	
Titanium	0.0005	0.0009
Tiodize	0.0004	0.0004
Z93C55		

Figure 7. Hoekstra-Voight coefficient plot shown for Tiodize type II-coated titanium under vacuum conditions and tabulated Hoekstra-Voight coefficients for all calculated materials

IV. Conclusion

These data and tests demonstrate the efficacy and ease at which qualitative and quantitative measures of adhesive force can be calculated on lunar simulant. The testing hardware and experimental setup can be used for nearly any material that is desired to be tested. Sample holders can be readily printed with difference sized notches to tolerate a variety of sample sizes, although the 1.5 cm x 3 cm sample coupon seems to be of an appropriate size to facilitate high throughput testing.

The data shown in this work agrees with previous efforts at determining the adhesive force of lunar simulant. While exact quantities may not be identical, the trends that govern their differences are, indicating appropriate experimental design and valid results. Additionally, many of the differences can be explained through the increased fidelity of this work as compared to those prior.

However, there are numerous improvements that can be made to the hardware and its capabilities should this test progress. To increase the homogeneity of the simulant application, a taller simulant application mechanism, coupled with an analogous taller hard stop, could be installed. The increased height of the simulant application mechanism would allow for a more even distribution of simulant across the samples. Additionally, adding the simulant with an increased rotational speed with this added height should apply a less concentrated areal density of simulant on the sample, further decreasing any potential cohesion or simulant ejection "avalanching" at low rotational speeds. Preliminary test data has shown that the existing hardware and operation are able to repeatably provide a percent surface area coverage of ± 5% (see Section II.B). It is expected that further improvements in the design will be able to halve this range.

Incorporating the ability to apply or quantify charge on the simulant would additionally increase fidelity. It is known that the dust on the lunar surface will be highly charged, and so hardware and its capabilities should be designed to integrate these characteristics into the experimental design [14]. While numerous methods to include this capability have been informally proposed, it is not known if any have been demonstrated to work in an analogous test. Additionally, attempts should be made to introduce a plasma environment into the vacuum chamber since the lunar surface has a well-known, though not necessarily well-characterized, plasma environment. [15].

The last included, though certainly not final, upgrade to the hardware involves an improvement or addition in the ability to obtain mid-test or *in situ* measurement of the particle size distribution of the ejected simulant. While preliminary tests showed that test-to-test variance is low, it was not zero, indicating that some imprecision was added to the test when removing, measuring, and cleaning the samples between each run. With the existing hardware and infrastructure, the only known method to obtain the particle size distribution of the remaining simulant on the sample

was to remove the sample from the chamber, measure it under the microscope, clean it, place it back in the chamber, and repeat the process. The addition of an *in-situ* measurement tool, such as a precision high-speed camera, to track the simulant particles as they are ejected from the sample will enable this needed real-time measurement.

Acknowledgments

We would like to thank Valerie Wiesner and Chris Wohl, both of NASA's Langley Research Center, for the engaging discussions about various methods to test lunar simulant adhesion as well as their introduction of the Hoekstra-Voight Coefficient.

References

[1] D. Barker, A. Olivas, B. Farr, X. Wang, C. Buhler, J. Wilson and J. Mai, "Adhesion of lunar simulant dust to materials under simulated lunar environment conditions.," *Acta Astronautica,* vol. 199, pp. 25-36, 2022.

[2] E. L. Walton and C. S. Shaw, "Understanding the textures and origin of shock melt pockets in Martian meteorites from petrographic studies, comparisons with terrestrial mantle xenoliths, and experimental studies," *Meteoritics & Planetary Science,* pp. 55-76, 2009.

[3] R. Li, Y. Cui, Y. Feng, J. Wang, W. Huang, Y. Sui and D. Ren, "New mechanical models to study the impact of contact, wear, and adhesion of lunar dust on space materials," vol. 15, no. 4, 2023.

[4] National Aeronautical and Space Administration, "Classification and Requirements for Testing Systems and Hardware to be Exposed to Dust in Planetary Environments: NASA-STD-1008," NASA, Houston, 2021.

[5] R. G. Lee and G. L. Brown, "Overview of NASA Gateway Lunar Dust Mitigation and Contamination Modeling and Analysis," 2023.

[6] A. Dove, G. Devaud, X. Wang, M. Crowder, A. Lawitzke and C. Haley, "Mitigation of lunar dust adhesion by surface modification," *Planetary and space science,* pp. 1784-1790, 2011.

[7] R. G. Lee, E. S. Worthy, E. M. Willis, G. L. Brown, F. Cipriani and D. C. Barker, "Development of a comprehensive physics-based model for study of NASA gateway lunar dust contamination," *Acta Astronautica,* vol. 210, pp. 616-626, 2023.

[8] B. .. Yilbas, A. Al-Sharafi, H. Ali, N. Al-Aqeeli, H. Al-Qahtani, F. Al-Sulaiman, N. Abu-Dheir, G. Abdelmagid and A. Elkhazraji, "Environmental dust removal from inclined hydrophobic glass surface: avalanche influence on dynamics of dust particles," *RSC Advances,* vol. 8, no. 59, pp. 33775-33785, 2018.

[9] K. A. Alshibli and A. Hasan, "Strength properties of JSC-1A lunar regolith simulant," *Journal of Geotechnical and Geoenvironmental Engineering,* vol. 135, no. 5, pp. 673-679, 2009.

[10] C. S. Ray, S. T. Reis, S. Sen and J. S. O'Dell, "JSC-1A lunar soil simulant: Characterization, glass formation, and selected glass properties," *Journal of Non-Crystalline Solids,* vol. 44, no. 49, pp. 2369-2374, 2010.

[11] X. Zeng, C. He, H. Oravec, A. Wilkinson, J. Agui and V. Asnani, "Geotechnical properties of JSC-1A lunar soil simulant," *Journal of Aerospace Engineering,* vol. 23, no. 2, pp. 111-6, 2010.

[12] R. T. Fox, J. H. Litofsky, S. R. Nagpal, M. A. Prado and S. A. Lee, "Lunar Dust Fates in the HLS Crew Compartment: Novel Experimental and Analytical Characterization and Techniques," *in prep,* 2025.

[13] R. F. Scott and K. A. Zuckerman, "Examination of returned Surveyor III surface sampler," *Proceedings of the Lunar Science Conference, vol. 2,* vol. 2, p. 2743, 1971.

[14] J. J. Rennilson and D. R. Criswell, "Surveyor observations of lunar horizon-glow," *The Moon,* vol. 10, no. 2, pp. 121-142, 1974.

[15] R. H. Manka, "Plasma and potential at the lunar surface," *Proceedings of the 6th Eslab Symposium,* pp. 347-361, 1972.